IJDACR
ISSN: 2319-4863

IJDACR
International Journal Of Digital Application & Contemporary Research

International Journal of Digital Application & Contemporary Research
Website: www.ijdacr.com (Volume 4, Issue 1, August 2015)

Evaluating Path Loss Models for E-Band Communication

Prakash Yadav
M. Tech. Scholar
Mahakal Institute of Technology, Ujjain, M. P. (India)

Mohit Pant
Associate Professor
Mahakal Institute of Technology, Ujjain, M. P. (India)

Abstract – **The allocation of a large amount of bandwidth by regulating bodies in the 70/80 GHz band, i.e., the E-band, has opened up new potentials and challenges for providing affordable and reliable Gigabit per second wireless point-to-point links. This paper gives a comparative analysis of pathloss for different frequency bands of the respective path loss models. Subsequently, different propagation models, ITU-R and SUI models, are compared against measurement results and it is concluded that to meet specific availability requirements, E-band wireless systems may need to be designed with larger fade margins compared to microwave systems.**

Keywords– **E-Band, Pathloss, ITU-R, SUI.**

I. INTRODUCTION

The popularity of multimedia applications and broadband internet has created an ever increasing demand for achieving higher throughputs in cellular and wireless networks. Thus far, wireless point-to-point links have been playing an important role in carrying a large portion of this data by interconnecting cellular base stations or enterprise buildings. In fact, due to their low cost of installation and insusceptibility to environmental effects, more than fifty percent of today's cellular base stations are interconnected using wireless backhaul links [1]. Yet, if wireless point-to-point links are expected to continue to be widely applied in next generation cellular networks, they have to support throughputs comparable to that of fiber-optic links. This task is made difficult by the limited bandwidth available in the microwave band [2]. In this regard, the large bandwidth available in the 70 and 80 GHz or E-band has opened up new opportunities for developing multi-Gigabit per second (Gbps) wireless links [1, 3].

Even though the available bandwidth in the E-band is more than fifty times the entire cellular spectrum, radio signals in the E-band are more adversely affected by environmental factors [4]. The characteristics of E-band signals and systems can be summarized as follows:

- Due to the higher carrier frequencies, the antennas are more directional making E-band systems mainly suitable for line-of-sight (LOS) applications.
- Rain and obstacles more severely attenuate radio signals in the E-band. Consequently, with the same transmit power and link availability requirements, E-band wireless links can operate over shorter distances when compared to microwave systems. For example, let us consider two point-to-point wireless systems with a 99:999% availability requirement and a fade margin of 0 dB: the first system operating at 23 GHz and employing 256-quadrature amplitude modulation (QAM) can achieve a link distance of 3 kms at 1:4 Gbps, while the second system utilizing the 70/80 GHz spectrum and using binary phase shift keying (BPSK) can only operate over 1:9 kms at 3 Gbps [4].
- To achieve the high carrier frequencies required by E-band systems, a voltage controlled oscillator's signal needs to be taken to E-band carrier frequencies using a larger frequency multiplication factor compared to systems operating in the microwave band. This, in turn, can result in larger oscillator phase noise variances. Phase noise, which is present in communication systems due to imperfect oscillators, can significantly impact their bandwidth efficiency and performance, since it results in the rotation of the signal constellation from one symbol to the next symbol [5]. Moreover, in E-band systems, due to the LOS nature of the links, the coherence time of the channel is much longer compared to the phase noise variation time. This means that phase noise can be a performance bottleneck in E-band systems whilst in other systems the channel variations might be the fundamental limitation.
- Because of the received signal's large bandwidth and high sampling rate,E-band systems require the application of high speed digital signal processing, digital-to-analog conversion (D/A), and analog to- digital conversion (A/D) units at the transceivers.
- Due to the very high carrier frequencies, the power amplifiers used in E-band systems have a very limited output range and are inefficient compared to those employed in the microwave band. Hence, the output power levels of most existing E-band systems are lower than the

IJDACR
ISSN: 2319-4863

IJDACR
International Journal Of Digital Application & Contemporary Research

International Journal of Digital Application & Contemporary Research
Website: www.ijdacr.com (Volume 4, Issue 1, August 2015)

maximum levels allowed by regulating bodies. This further limits the operating range of these systems.

Because of these limitations, thus far, most E-band systems use low order modulations such as BPSK and on-off keying, and are not spectrally efficient compared to traditional microwave links. In fact, current E-band systems achieve a spectral efficiency of 0:5–2:4 b/s/Hz [6], whereas the spectral efficiencies of traditional microwave systems are in the range of 4–12 b/s/Hz [7].

To enable the development of multi-Gbps wireless links, it is paramount to introduce new transceiver designs for E-band systems that can more efficiently utilize the available bandwidth, while supporting wireless links over distances comparable to those of microwave links. To this end, this article first reviews the bandwidth allocation and licensing in the E-band. Next, unlike previous articles that did not take into account the effect of phase noise [6], [8], by comparing measurement results with the current models for signal attenuation and oscillator phase noise, it is shown that traditional models developed for the microwave band may not accurately predict these phenomena in the E-band.

The development of more accurate models is anticipated to result in better link budget planning and more accurate tracking of phase noise, which can in turn enhance the bandwidth efficiency of E-band systems, e.g. enabling the application of higher order modulations. Subsequently, a new multi-input multi-output (MIMO) transceiver design is outlined and new topologies and applications for E-band systems are proposed that can mitigate their limitations and better utilize their potential. The main objective of this paper is to study concepts of wireless communication with effect of multi path propagation over radio link. This paper also calculate the path loss during the transmission of radio waves.

II. Channel and Phase Noise Models for the E-Band

Accurate channel and oscillator phase noise models for the E-band spectrum are essential for link budget planning and accurate tracking of phase noise in E-band systems. Both of these improvements are expected to enhance the bandwidth efficiency of E-band systems in the near future [7]. Thus, in this section, we examine the accuracy of the existing models for both phenomena in the E-band.

Characteristics of E-Band

To accurately predict the effect of environmental conditions on the performance of wireless communication systems, the ITU-R and Crane models have been extensively applied for link-budget planning in the microwave band. In order to determine the accuracy of these models in predicting rain intensity and the resulting signal attenuation in the E-band, a long term measurement campaign was carried out in Gothenburg, Sweden, by Ericsson Research, where the rain intensity and the signal attenuation of an E-band system was measured over a period of nine months [9]. The results of this measurement campaign and a comparison with respect to both the ITU-R and Crane models are plotted in Figure 1.

It can be observed that both the ITU-R and Crane models can rather sufficiently predict the rain intensity in this region, since the signal attenuation calculated based on the measured rain intensity is close to that of the ITU-R and Crane models. However, the measurement results in Figure 1 show that the measured signal attenuation in the E-band is considerably higher than the attenuation predicted by both the ITU-R and Crane models.

This demonstrates that both models, which are well suited for the microwave band, are not capable of accurately predicting the channel attenuation in the E-band. Thus, for E-band wireless point-to-point links to meet the expected 99:999% availability requirements, the fade margin needs to be chosen larger than the values calculated using the Crane and ITU-R models, e.g. 5–10 dB higher as shown in Figure 1.

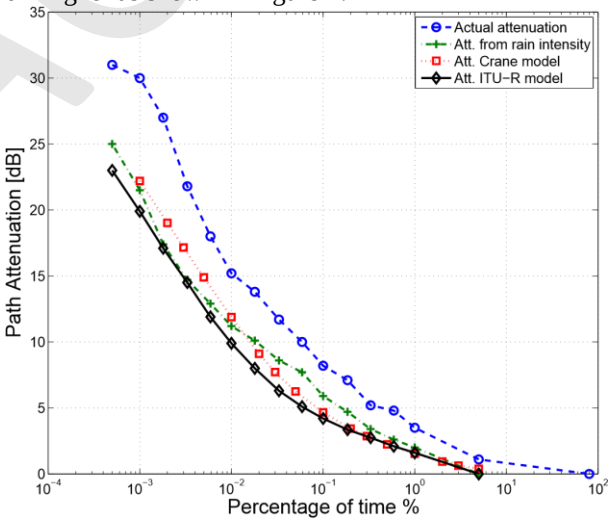

Figure 1: Path attenuation versus time plot with transmit power=18:6 dBm, receiver threshold= –58 dBm, antenna gain=43 dBi, Tx/Rx separation=1 km±50 m, data rate=1:25 Gbps, differential BPSK (the measurements are also reported in [9]) [10]

This new finding indicates that to avoid larger than necessary fade margins, more accurate channel attenuation models have to be developed for the E-band. These more accurate channel and propagation models are also anticipated to enhance the bandwidth efficiency of E-band systems.

Note that although the shortcomings of the ITU-R model in predicting the attenuation for E-band systems has also been confirmed in [8], in this work, for the first time, we

IJDACR
ISSN: 2319-4863

IJDACR
International Journal Of Digital Application & Contemporary Research

International Journal of Digital Application & Contemporary Research
Website: www.ijdacr.com (Volume 4, Issue 1, August 2015)

present a comparison with respect to the Crane attenuation model, which is more extensively applied in North America [8].

Phase Noise Models in E-Band

One of the main challenges in E-band communication systems is to equip the transceivers with low phase noise high-frequency oscillators. Nevertheless, recent studies have shown that such oscillators may be designed using Gallium-Nitride technology, waveguide theory, and opto-electronic techniques [11], [12]. Generally, two methods are proposed to generate high-frequency oscillation [11], [12]. One is to design an on-chip high-frequency oscillator and the other is to increase the frequency of a low-frequency oscillator by means of frequency multipliers.

Even though the former is expected to result in more accurate oscillators, research has shown that the design of accurate and affordable oscillators for commercial applications via this approach is a challenging task. On the other hand, the latter approach increases a low-frequency oscillator's phase noise variance by the so-called multiplication factor [11]. As a result, oscillator phase noise is one of the main limiting factors in the application of higher order modulations in E-band systems [4].

Although the effect of oscillator phase noise in narrowband systems has been extensively studied, there is a lack of understanding of this impairment for the wideband systems deployed in the E-band. According to traditional phase noise models, the phase noise variance or rate is linearly proportional to the sampling time applied at the receiver [5]. Therefore, it is expected that systems employing larger bandwidths and smaller sampling times will experience a smaller phase noise variance. However, by increasing the signal bandwidth, other system parameters such as the bandwidth of the receiver front-end filter must also be increased. Consequently, this leads to an increase in phase perturbation introduced to the entire communication system.

To illustrate this effect in wideband systems, Figure 2 depicts the measured power spectral density (PSD) of oscillator phase noise for a monolithic microwave integrated circuit oscillator operating at 9:9 GHz. Figure 2 compares measurement results with the traditional Wiener phase noise model, which is extensively applied for the microwave band. Note that unlike the traditional phase noise models, the phase noise PSD of an oscillator does not continue to decrease with increasing offset frequency. In fact, as shown in Figure 2, in practice, the phase noise PSD exhibits a floor region beyond a certain offset frequency. Thus, as the bandwidth of a communication system increases, the floor region in the PSD of an oscillator is expected to play an important role in the overall system's performance.

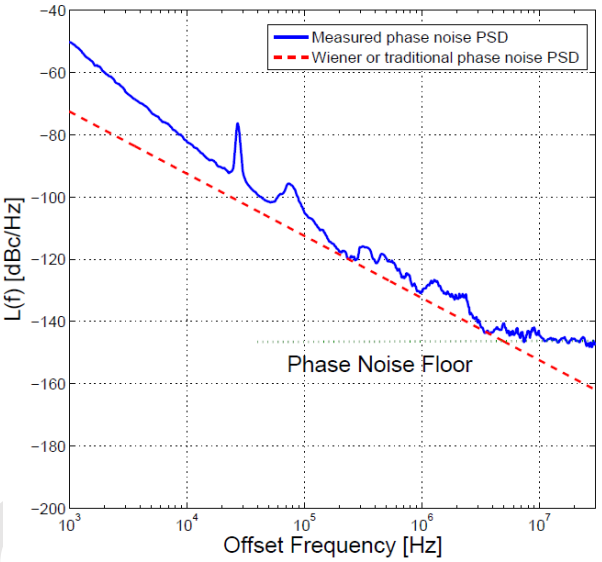

Figure 2: The power spectral density of a free-running oscillator operating at 9.9 GHz [10]

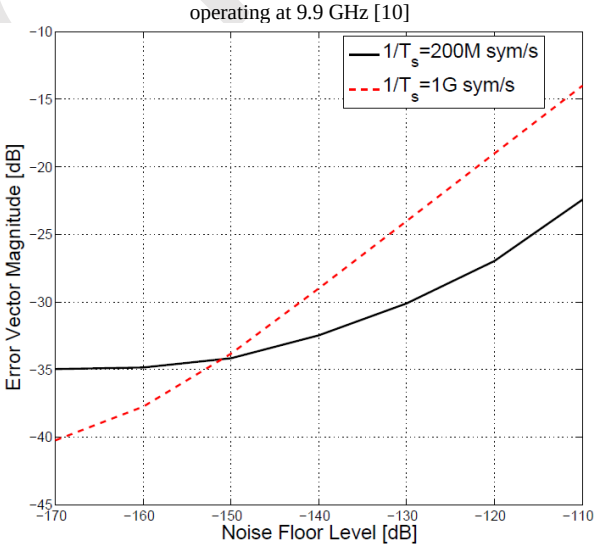

Figure 3: EVM of residual phase noise error for two systems with different symbol rates v/s oscillator phase noise floor power [10]

To verify this finding, in Figure 3, the performances of two communication systems with different bandwidths are compared in terms of the error vector magnitude (EVM) (also known as receive constellation error) for different phase noise floor levels (signal-to-noise ratio (SNR)= 30 dB and 16-QAM). Figure 3 shows that below a certain noise floor level, the cumulative phase noise is dominant and a system with higher symbol rate experiences a lower EVM. However, as the phase noise floor increases, the performance of a communication system employing a larger bandwidth degrades more dramatically. It is also important to consider that due to

IJDACR
ISSN: 2319-4863

IJDACR
International Journal Of Digital Application & Contemporary Research

International Journal of Digital Application & Contemporary Research
Website: www.ijdacr.com (Volume 4, Issue 1, August 2015)

the use of frequency multipliers, it is expected that most oscillators used in E-band systems have higher phase noise floor levels. For example, if the above 9:9 GHz oscillator is used in an E band system operating at 70 GHz, a frequency multiplier with a multiplication factor of 7 needs to be applied, which will increase the noise floor by 20 log 7 = 16:9 dBc.

Therefore, from the results in Figures 2 and 3, it can be concluded that the phase noise models that are used for narrowband systems, e.g., the Wiener model, cannot be applied to accurately predict the properties of this impairment in wideband systems. Thus, more accurate phase noise models for wideband communication systems have to be developed to estimate and compensate the effect of phase noise more effectively, which in turn enables the use of more bandwidth-efficient modulation schemes.

III. MIMO Transceiver Design for E-Band Systems

The development of MIMO technology has been largely based on the assumption of rich multipath which combined with the deployment of multiple antennas results in multiple independent spatial channels between two terminals. Under these circumstances, it has been theoretically shown that the MIMO system capacity scales linearly with the minimum of the number of transmit and receive antennas. However, E-Band systems are expected to operate under strong LOS conditions, thereby creating several research challenges and opportunities for the design of efficient E-band MIMO transceivers [3], [13], [14]. More importantly, the antenna properties in the E-band are attractive for three important reasons:

- They result in high antenna gains for a given antenna size.
- They enable highly directional communication with narrow beams, thus, reducing interference, and
- They support the deployment of large-dimensional MIMO systems with relatively compact antenna arrays.

Two benchmark E-band systems dominate the current state-of-the-art. In the first configuration, termed a DISH system, conventional continuous aperture “dish” antennas are used in highly directional LOS point-to-point links. Such systems are currently used for wireless backhaul links, e.g., in the commercial systems offered by Siklu, E-band Communications, or Bridge wage.

In the second configuration, termed conventional MIMO, the antenna elements are placed sufficiently far apart so that the spatial LOS responses become independent. The required antenna spacing can be worked out via simple geometrical arguments, and leads to the so-called Rayleigh spacing. For a given transmitter-receiver distance, the Rayleigh antenna spacing is inversely proportional to the carrier frequency. Thus, compared to microwave systems, LOS MIMO technology is more suitable for E-band systems, since the antenna spacing is smaller and the transceivers can be housed within a relatively compact module. However, while such systems can exploit multiplexing gains, they suffer from poor power efficiency and increased interference [13]. In principle, the above limitations of conventional MIMO systems can be eliminated by using half-wavelength spaced large antenna arrays. Although such systems can optimally exploit the spatial dimension, they suffer from a prohibitively high transceiver complexity due to the requirement of a large number of array elements. For example, a 600 planar array operating at 80 GHz requires about 6400 antenna elements, while each antenna element requires a dedicated transceiver module [13]. Recall that propagation in the E-band is expected to have sparse multipath components and is predominantly LOS. Thus, the spatial multiplexing gain of a MIMO E-band system can, in practice, be much smaller than the minimum of the number of transmit and receive antennas employed. In other words, compared to a system in the microwave band, the spatial communication subspace for a MIMO E-band system can be expressed with a smaller number of orthogonal basis functions [3], [13]. Accordingly, to fully exploit the potential of MIMO technology and to reduce the transceiver complexity, the number of beams transmitted or received by a MIMO E-band system needs to be equal to the dimensionality of the E-band channel subspace. This characteristic of E-band channels has motivated the development of the CAP-MIMO transceiver.

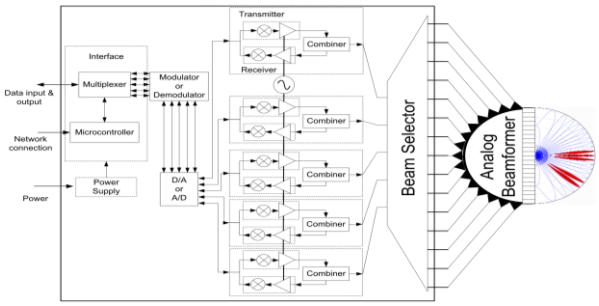

Figure 4: Radio unit for an E-band CAP-MIMO system [10]

CAP-MIMO combines the multiplexing gain of MIMO systems, the antenna gain of DISH systems, and the beam forming capability of phased arrays to optimally exploit the smaller spatial dimensionality at E-band frequencies [13]. CAP-MIMO uses a high-resolution discrete lens array to perform analog beam forming in the pass band, see Figure 4. Essentially, in this setup, a relatively small

IJDACR
ISSN: 2319-4863

IJDACR
International Journal Of Digital Application & Contemporary Research

International Journal of Digital Application & Contemporary Research
Website: www.ijdacr.com (Volume 4, Issue 1, August 2015)

number of active beams are radiated by the corresponding feed antennas on the focal surface of the lens array. The number of transmitted beams is directly proportional to the dimensionality of the communication channel.

This approach ensures that the CAP-MIMO transceiver is equipped with the smallest number of A/D, D/A, and radio frequency units, while fully taking advantage of the potential of MIMO technology. Figure 4 depicts the radio unit for a CAP-MIMO system. In this setup, it is assumed that 5 spatially independent channels can be established between transmitter and receiver. Consequently, the CAP-MIMO system only requires 5 transceiver blocks. The beam selector block in Figure 4 ensures that appropriate beams are selected for signal transmission and reception, which is analogous to an antenna selection block in a conventional MIMO system.

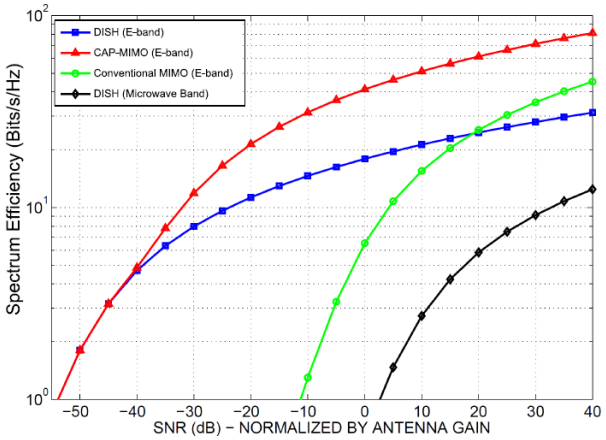

Figure 5: Bandwidth efficiency comparison of CAP-MIMO, conventional MIMO, and DISH systems [10]

IV. PROPOSED METHODOLOGY

SUI Model for UHF/Microwave Band

Path loss, which dictates the RF coverage distance (i.e., cell size) for cellular systems employing omni directional antennas, is generally inversely proportional to the square of the carrier frequency, as modeled by the Friis free space path loss formula [15]. In cellular planning, path loss must be estimated for a deployment environment, and cell coverage is determined based on the base station (BS) and mobile station (MS) antenna gains, effective isotropic radiated power (EIRP), RF bandwidth, and modulation and coding techniques. Omnidirectional large-scale path loss in urban environments may be estimated from the Hata model and the COST231 extension of the Hata model for carrier frequency (*fc*) below 2 GHz [16], and from the SUI model for *fc* above 2 GHz:

$$PL_{SUI}(d) = PL(d_0) + 10nlog_{10}10\left(\frac{d}{d_0}\right) + X_{fc} + X_{RX} + X_{\sigma} \quad (1)$$

Where,

$$PL(d_0) = 20log_{10}(\frac{4\pi d_0}{\lambda}) \quad (2)$$

$$n = a - b.h_{TX} + \frac{c}{h_{TX}} \quad (3)$$

$$X_{fc} = 6.log_{10}\left(\frac{f_{MHz}}{2000}\right).f_c > 2GHz \quad (4)$$

$$X_{RX} = -10.8.log_{10}(\frac{h_{RX}}{2}) \quad (5)$$

λ is the carrier wavelength in meters, $PL(d_0)$ in equation (2) denotes the free space path loss in dB at a close-in reference distance d_0; X_{fc}, and X_{XR} in equation (5) denote the correction factors for frequency and receiver heights, respectively, and X_{σ} in equation (1) is the typical lognormal random shadowing variable with 0 dB mean and standard deviation σ [dB] such that 8.2 < σ < 10.6 dB [17]. *f*MHz in equation (4) is the carrier frequency (*fc*) in MHz; h_{TX} and h_{RX} denote the transmitter (TX) and receiver (RX) antenna heights in meters, respectively.
The parameters *a*, *b*, and *c* in equation (4) are constants used to model the terrain types encountered in the service area. Here we consider the model suited for hilly and dense vegetation (denoted SUI terrain type *A*), with parameters given as *a* = 6, *b* = 0.0075, and *c* = 12.6 [17]. The path loss model in equation (1) is used for cellular systems in many markets throughout the world.

Proposed ITU-R Model

Free-space loss is proportional to the square of the operating frequency; therefore, the free space loss in the 60/70/80/95/120 GHz bands is much higher than the losses in the 2.4 GHz or 5 GHz bands available in many administrations for WLAN operations.
The free-space loss PLFS (dB) at a reference distance d_0(m) is given by:

$$PL_{FS} = 20\ \log_{10}\left(\frac{4\pi\ d_0}{\lambda}\right) \quad (6)$$

Where λ is the wavelength (m). The average path loss over a distance d (m) can be determined using the following path loss exponent model based on Recommendation ITU-R P.675 (ex-CCIR):

$$\overline{PL}(d) = PL_{FS}(d_0) + 10\ n\ \log_{10}\left(\frac{d}{d_0}\right) \quad (7)$$

Where:

$\overline{PL}(d)$: the average path loss (dB) at a particular distance d

IJDACR
ISSN: 2319-4863

IJDACR
International Journal Of Digital Application & Contemporary Research

International Journal of Digital Application & Contemporary Research
Website: www.ijdacr.com (Volume 4, Issue 1, August 2015)

n: the path loss exponent that characterizes how fast the path loss increases with transmit and receive antenna separation.

Figure 6 shows the simulated results of the received signal level (dBm) as a function of the distance from the transmit antenna. The simulated results are provided for the 2.4/5.5/60/70/80/95/120 GHz bands. In this simulation, it is assumed the transmit power P_t is 10 dBm, the transmit and receive antenna gains (G_t and G_r) are unity, n is 2.1, and the oxygen absorption is 15 dB/km for the 60 GHz band and zero otherwise.

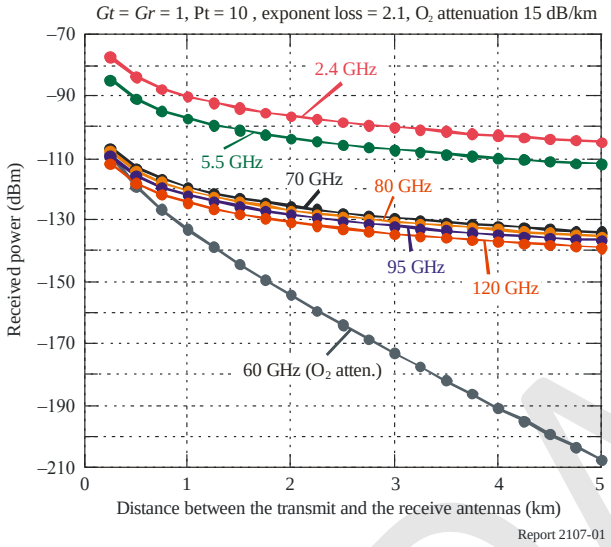

Figure 6: Received power (dBm) vs. distance (km)

From Figure 6, the path loss at 60 GHz is much higher than the losses at other frequency bands because of the oxygen absorption, which is detrimental to signal propagation. In an outdoor environment, the gaseous absorption attenuates the transmitted signal (~10 to 15 dB/km) in addition to free-space loss. Notwithstanding the above, the oxygen absorption loss can be compensated for by the use of high-gain directive antennas. As well, it can also prove attractive for short-range communications as it further attenuates harmful interference such as co-channel interference in wireless cell-based systems, which combined with low transmit powers in the 60 GHz band (~10 mW) can increase frequency reuse from cell to cell.

For the 70/80/95/120 GHz bands, the gaseous absorption is negligible. Figure 7 shows the attenuation (dB/km) vs the frequency (GHz) due to the gasses and hydrometeors for radio transmission through the atmosphere. The figure indicates that rain has the greatest impact on transmitted signals in the 60/70/80/95/120 GHz bands.

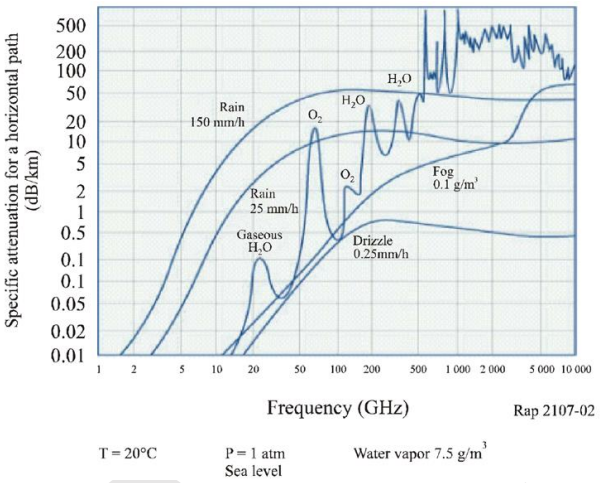

Figure 7: Attenuation due to gasses and hydrometeors for transmission through the atmosphere

Therefore, enhancement of RF devices and techniques in these frequency bands would improve the availability of these networks under rainy conditions.

For indoor applications, transmitted signals in the 60/70/80/95/120 GHz bands are significantly attenuated by surrounding objects and inner walls and can result in a substantial drop in the received signal level.

Additionally, measured values of RF signal material attenuation have been published in [15]. The following results of minimum and maximum attenuation (57-95 GHz) through various materials have been interpolated from these findings:

- Fibreglass insulation: ~3-3.5 dB
- Dry paper-towel: ~3-3.5 dB
- Asphalt shingle: ~3.5-4 dB
- Drywall: ~3.5-6.5 dB
- Glass: ~5-7 dB
- Wet paper-towel: ~5-7 dB
- 19 mm pine board: ~8-11 dB
- 19 mm plywood: ~7-11 dB
- Clay brick: 10-23 dB
- Painted 2 × 8 (5 cm × 20 cm) board: ~20-35 dB.

There are also various ITU-R Recommendations that are useful in dealing with propagation issues at these frequencies.

Other factors such as delay spread and Doppler may also need to be taken into consideration. The delay spread is caused by reflections and scattering and will depend on the size of the room and the nature of the walls and objects in it. In a typical office (nomadic) environment, the reflected signals may cause delay spread of the order of few tens of nanoseconds at 58 GHz and subsequence intersymbol interference, depending on the symbol duration. This effect can be minimized by using directive antennas, which in turn complicate other aspects such as broader coverage.

IJDACR
ISSN: 2319-4863

IJDACR
International Journal Of Digital Application & Contemporary Research

International Journal of Digital Application & Contemporary Research
Website: www.ijdacr.com (Volume 4, Issue 1, August 2015)

Proposed CRANE Model

The Crane Model is a theoretical prediction model based on the geophysical observations of rain rate, rain structure, and the vertical variation of atmosphere temperature. The model is summarized in equation (8) through (10) [18].

$$A_R = aR^b \left[\frac{e^{ubd}-1}{ub}\right] \quad \text{(For } 0 \le D \le d\text{)} \quad (8)$$

$$A_R = aR^b \left[\frac{e^{ubd}-1}{ub} - \frac{B^b e^{cbd}}{cb} + \frac{B^b e^{cbD}}{cb}\right] \quad \text{(For } d \le D \le 22.5 \text{ km)} \quad (9)$$

Where,

$u = \ln[B\, e^{cd}]/d$

$B = 2.3\, R^{-0.17}$

$c = 0.026 - 0.03 \ln(R)$

$d = 3.8 - 0.6 \ln(R)$ km (10)

And A_R is path attenuation due to rain in dB, R is point rain rate in mm/hr and D is path length in km. For paths longer than 22.5 kms, the attenuation A_R is calculated for a 22.5km path and the resulting rain outage time is multiplied by a factor of (D/22.5). Multipliers a and b are rain attenuation coefficients dependent on frequency and polarization.

V. Simulation And Results

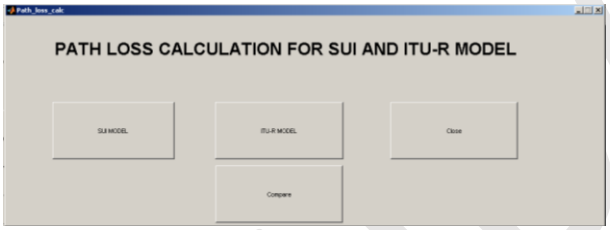

Figure 8: Graphical user interface for proposed approach

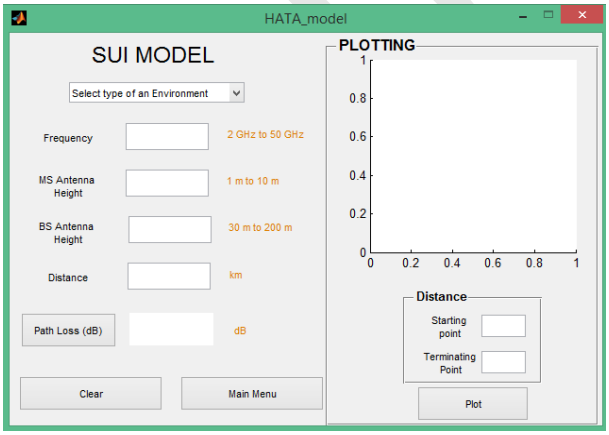

Figure 9: Graphical user interface of path loss calculation in SUI model

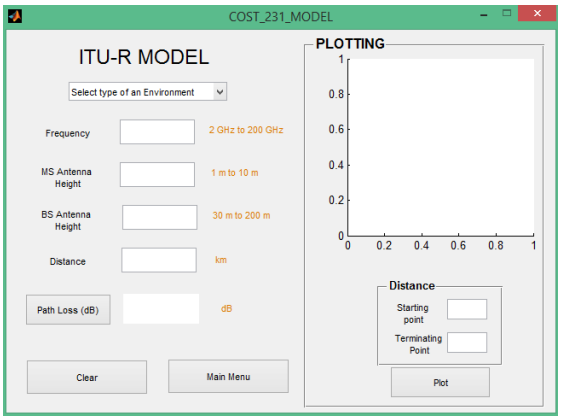

Figure 10: Graphical user interface of path loss calculation in ITU-R model

A comparative result analysis of path loss calculation for different frequency range is shows in following tables.

Table 1: Path loss calculation from 2 GHz to 100 GHz for Tx=5m and Rx=30m

Sr. No.	Tx Height	Rx Height	Distance	Frequency	Path Loss in SUI (dB)	Path Loss in ITU-R (dB)
1	5m	30m	5km	2ghz	83.1462	62.2262
2	5m	30m	5km	5ghz	91.5642	74.1484
3	5m	30m	5km	10ghz	98.6773	83.1673
4	5m	30m	5km	15ghz	102.59	88.443
5	5m	30m	5km	20ghz	105.3662	92.1862
6	5m	30m	5km	25ghz	107.5195	95.0896
7	5m	30m	5km	28ghz	108.6132	96.5642
8	5m	30m	5km	30ghz	109.2879	97.4619
9	5m	30m	5km	35ghz	110.7665	99.4676
10	5m	30m	5km	40ghz	112.0551	101.205
11	5m	30m	5km	45ghz	113.1917	102.7375
12	5m	30m	5km	50ghz	114.2084	104.1084
13	5m	30m	5km	55ghz	115.1282	105.3486
14	5m	30m	5km	60ghz	115.9678	106.4807
15	5m	30m	5km	65ghz	116.7402	107.5222
16	5m	30m	5km	70ghz	117.4554	108.4864
17	5m	30m	5km	80ghz	118.744	110.2239
18	5m	30m	5km	85ghz	119.329	111.0127
19	5m	30m	5km	90ghz	119.886	111.7564
20	5m	30m	5km	95ghz	120.4	112.4579
21	5m	30m	5km	100ghz	120.8	113.1237

Table 2: Path loss calculation from 2 GHz to 100 GHz for Tx=9m, Rx=185m and d=8km

Sr. No.	Tx Height	Rx Height	Distance	Frequency	Path Loss in SUI (dB)	Path Loss in ITU-R (dB)
1	9m	185m	8km	2ghz	76.2199	55.2999
2	9m	185m	8km	5ghz	83.3112	64.4712
3	9m	185m	8km	10ghz	88.6756	73.1656
4	9m	185m	8km	15ghz	91.8135	77.6665
5	9m	185m	8km	20ghz	94.0399	80.8599
6	9m	185m	8km	25ghz	95.7669	83.3369
7	9m	185m	8km	28ghz	96.6439	84.5949
8	9m	185m	8km	30ghz	97.1779	85.3608
9	9m	185m	8km	35ghz	98.3709	87.0719
10	9m	185m	8km	40ghz	99.4043	88.5542
11	9m	185m	8km	45ghz	100.3158	89.8617
12	9m	185m	8km	50ghz	101.1312	91.0312
13	9m	185m	8km	55ghz	101.8688	92.0892
14	9m	185m	8km	60ghz	102.5422	93.0551
15	9m	185m	8km	65ghz	103.1617	93.9436
16	9m	185m	8km	70ghz	109.7352	94.7663
17	9m	185m	8km	80ghz	104.7686	96.2485
18	9m	185m	8km	85ghz	105.2378	96.9215
19	9m	185m	8km	90ghz	105.6802	97.556
20	9m	185m	8km	95ghz	106.0986	98.1562
21	9m	185m	8km	100ghz	106.4956	98.7256

IJDACR
International Journal Of Digital Application & Contemporary Research

International Journal of Digital Application & Contemporary Research
Website: www.ijdacr.com (Volume 4, Issue 1, August 2015)

VI. CONCLUSION

The E-Band mobile communication technology for beyond 2020, will provide access to information and the sharing of data anywhere and anytime for anyone and anything. The model in this paper allows future realistic modeling of propagation conditions for millimeter wave transmission in urban and large size microcellular environments. This model also suggests that in future millimeter wave communications, mobile devices shall deploy antennas with higher gains and low noise to compensate for the additional path loss due to the frequency leap from low microwave to the millimeter wave region. It was found that the ITU-R model outperforms than the SUI model because the pathloss in SUI is greater than that of ITU-R model.

REFERENCES

[1] X. Huang, Y. J. Guo, A. Zhang, and V. Dyadyuk, "A multi-gigabit microwave backhaul," IEEE Commun. Mag., vol. 50, no. 3, pp. 122–129, Mar. 2012.
[2] J. Wells, "Faster than fiber: The future of multi-G/s wireless," IEEE Micr. Mag., vol. 10, no. 3, pp. 104–112, Mar. 2009.
[3] Z. Pi and F. Khan, "An introduction to millimeter-wave mobile broadband systems," IEEE Commun. Mag., vol. 49, no. 6, pp. 101–107, Jun. 2011.
[4] J. Wells, Multi-Gigabit Microwave and Millimeter-Wave Wireless Communications. Artech House, 2010.
[5] A. Chorti and M. Brookes, "A spectral model for RF oscillators with power law phase noise," IEEE Trans. Circuits Syst., vol. 53, no. 9, pp. 1989–1999, Sep. 2006.
[6] V. Dyadyuk, J. D. Bunton, and Y. J. Guo, "Study on high rate long range wireless communications in the 71-76 and 81-86 Ghz bands," in Proc. European Microwave Conf. (EuMC), pp. 1315–1318, Oct. 2009.
[7] Z. He, W. Wu, J. Chen, Y. Li, D. Stackenas, and H. Zirath, "An FPGA-based 5 Gbit/s D-QPSK modem for E-band point-to-point radios," in Proc. European Microwave Conf. (EuMC), Oct. 2011.
[8] L. Csurgai-Horvath, I. Frigyes, and J. Bito, "Propagation and availability on E-band terrestrial radio," in Proc. European Conf. Ant. Propag (EuCAP), pp. 73–75, Mar. 2012.
[9] J. Hansryd, L. Yinggang, J. Chen, and P. Ligander, "Long term path attenuation measurement of the 71–76 GHz band in a 70/80 GHz microwave link," in Proc. European Conf. Ant. Propag. (EuCAP), Apr. 2010.
[10] Mehrpouyan, Hani, M. Reza Khanzadi, Michail Matthaiou, Akbar M. Sayeed, Robert Schober, and Yingbo Hua, "Improving bandwidth efficiency in E-band communication systems,", Communications Magazine, IEEE 52, no. 3, pp. 121-128, 2014.
[11] P. Russer, "Si and SiGe millimeter-wave integrated circuits," IEEE Trans. Microw. Theory Tech., vol. 46, no. 5, pp. 590–603, May 1998.
[12] E. Ruscito, H. Chuang, R. Amaya, L. Roy, and B. Syrett, "A low cost oscillator for high data rate E-band transceivers," in Proc. Fly Wireless Work. (FBW), Jun. 2011.
[13] A. M. Sayeed and N. Behdad, "Continuous aperture phased MIMO: Basic theory and applications," in Proc. Allerton Conf. Control, Comput., Sep. 2010.
[14] F. Bøhagen, P. Orten, and G. E. Øien, "Design of capacity-optimal high-rank line-of-sight MIMO channels," IEEE Trans. Wireless Commun., vol. 4, no. 6, pp. 790–804, Apr. 2007.
[15] T. S. Rappaport, "Wireless Communications: Principles and Practice", 2nd ed., Prentice-Hall, 2002.
[16] Boccardi, Federico, Robert W. Heath, Aurelie Lozano, Thomas L. Marzetta, and Petar Popovski, "Five disruptive technology directions for 5G", Communications Magazine, IEEE 52, no. 2, 74-80, February 2014.
[17] P. D. Katev, "Propagation Models for Wimax at 3.5 GHz," IEEE-Elektro Conference, pp. 61–65, 2012.
[18] R. K.Crane, "Electromagnetic Wave Propagation through Rain", New York: John Wiley & Sons, 1996.